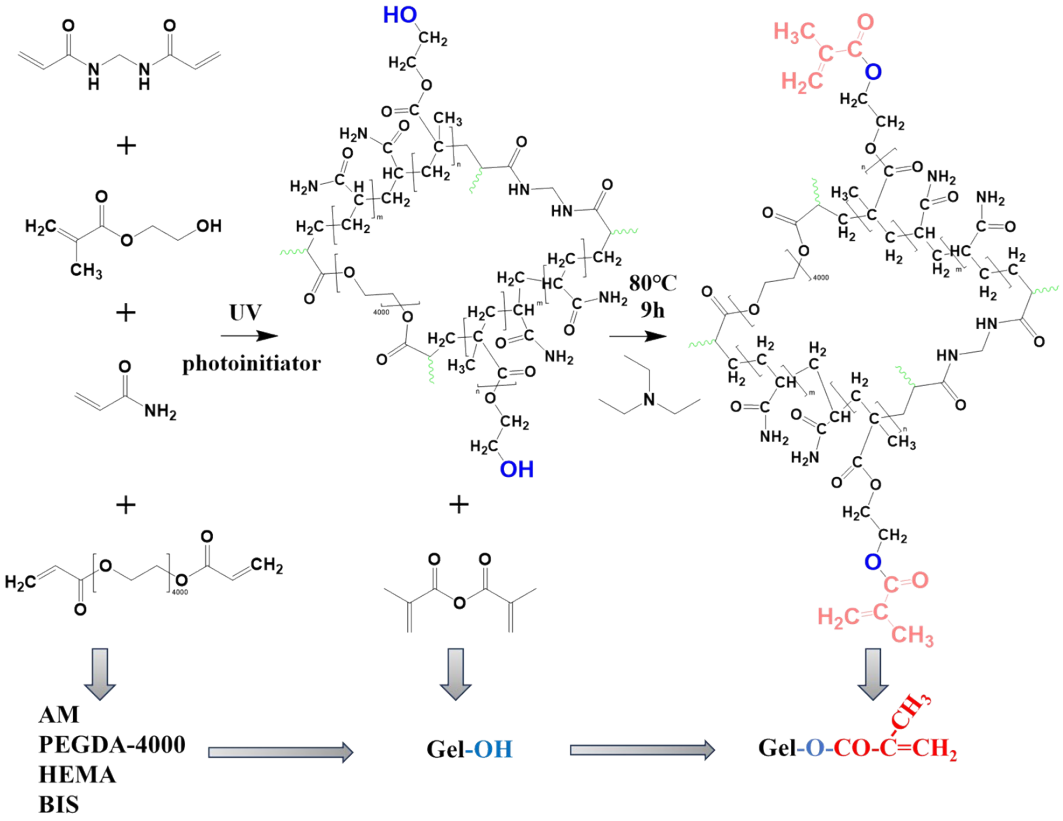

Figure S1. Reaction mechanisms of inverse opal film polymerization and modification.

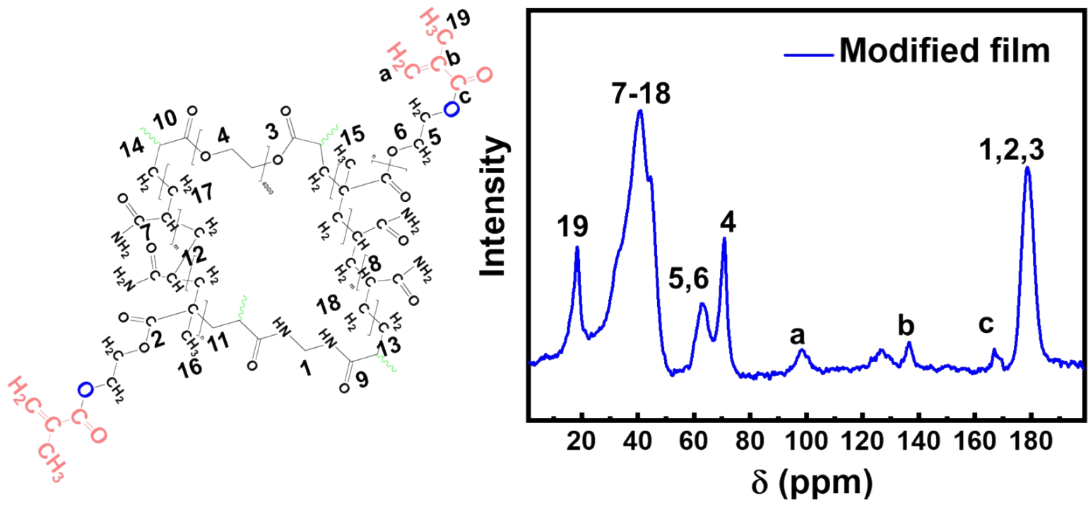

Figure S2. Chemical formulae and ^{13}C NMR of modified film.

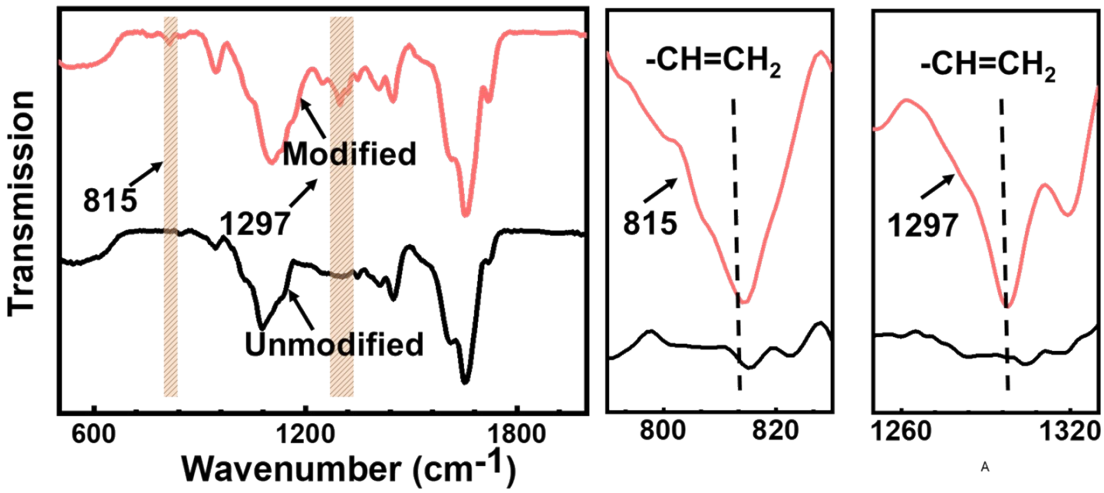

Figure S3. FT-IR of modified films and unmodified film (815 -C=CH_2 CH Out-of-plane bending vibration; 1297 -C=CH_2 in-plane bending vibration).

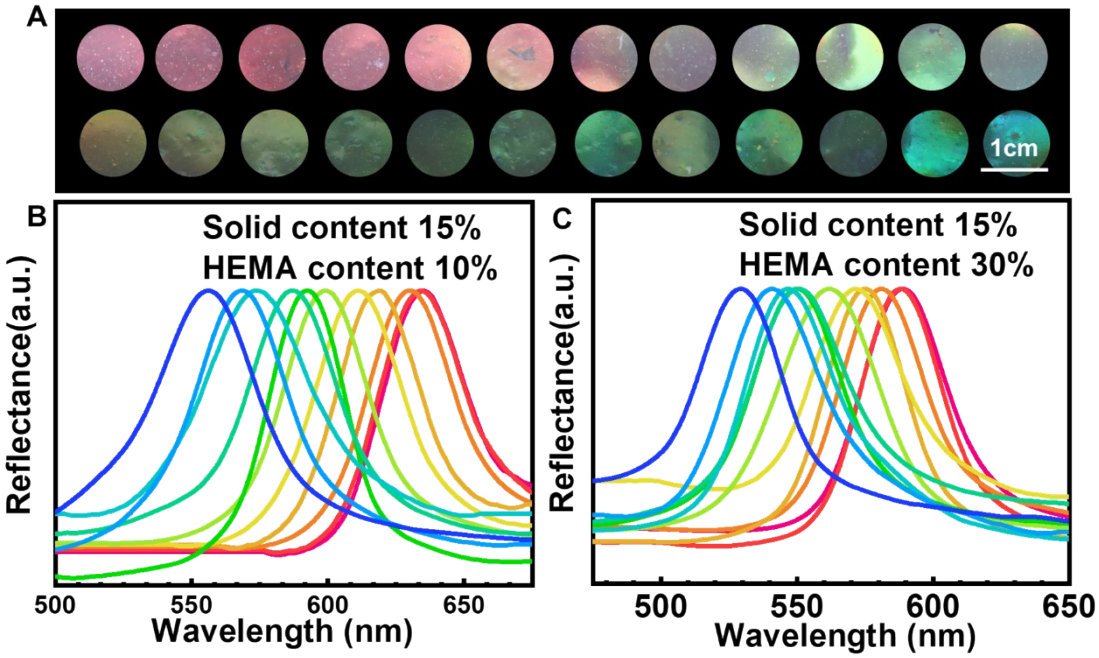

Figure S4. A Photographs of inverse opal films with solid content of 20% and acrylic groups content of 10% and 30% at different absorbed doses; **B** Spectra of inverse opal films with acrylic groups content of 10% and solid content of 15% at different absorbed doses; **C** Spectra of inverse opal films with acrylic groups content of 30% and solid content of 15% at different absorbed doses.

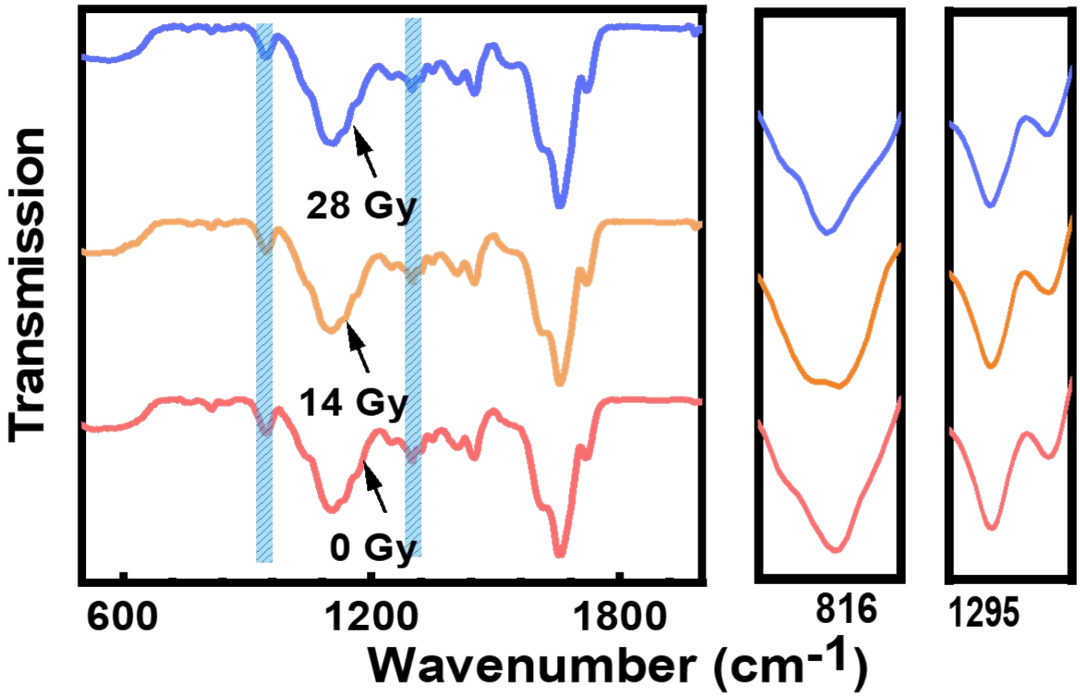

Figure S5. FT-IR of modified films with absorbed dose at 0, 10, 20 Gy and unmodified film (815 - $C=CH_2$ CH Out-of-plane bending vibration; 1297 -$C=CH_2$ in-plane bending vibration).

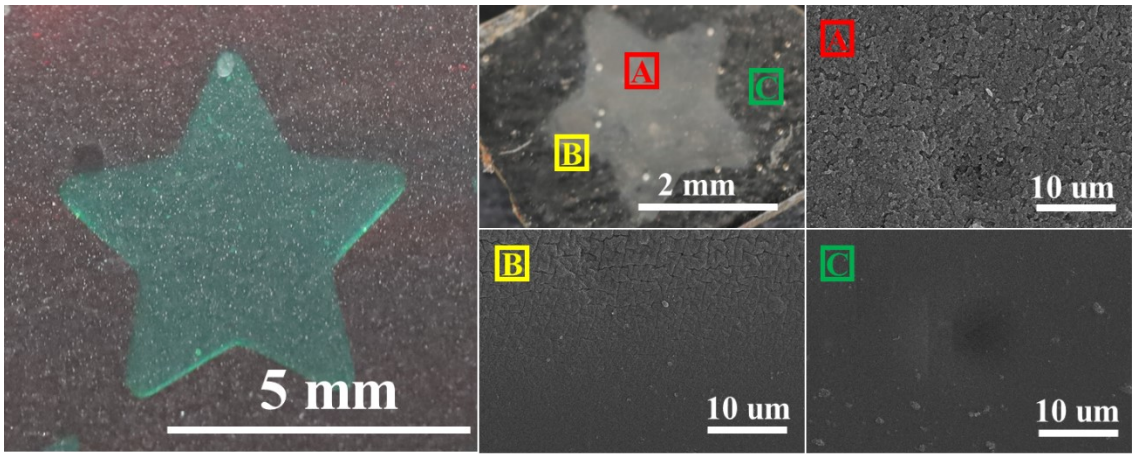

Figure S6. SEM images of different areas of the sample after drying.

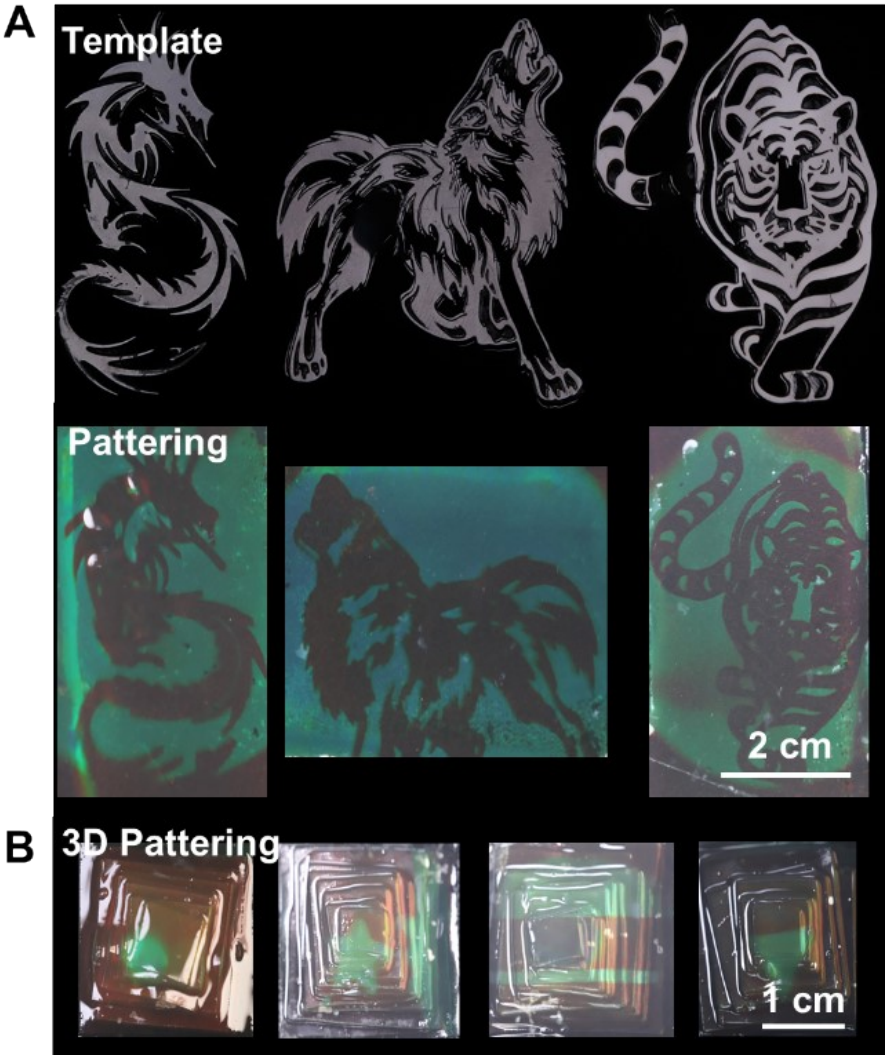

Figure S7. A Digital photo of films irradiated in the patterned radiation field; **B** 3D model of superimposed films and irradiated in different patterned radiation field.

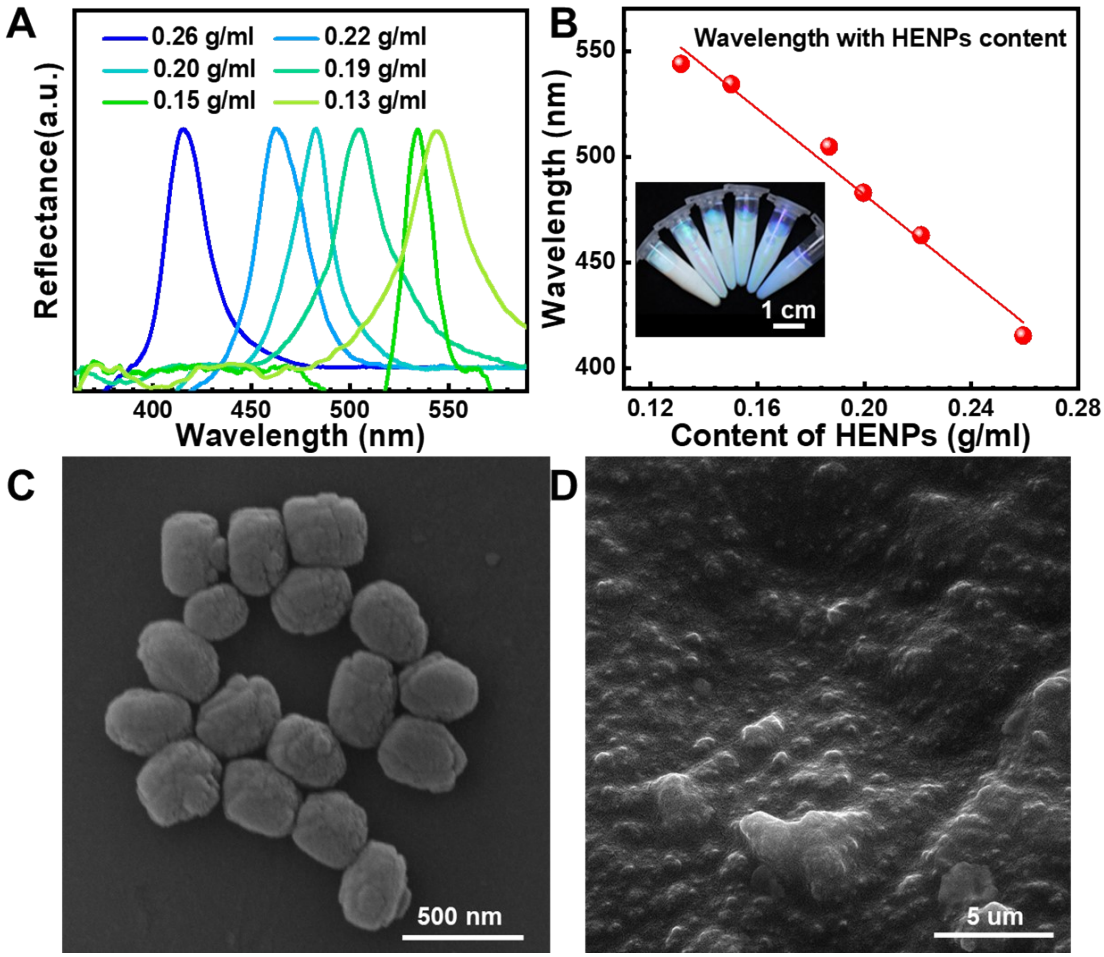

Figure S8. A The reflective spectrum of the HENPs with different mass volume fraction; **B** Linear fit of Bragg peaks wavelength with different mass volume fraction, with insets showing their corresponding Photographs; **C** SEM images of the HENPs; **D** SEM image of the HENPs in polymers.

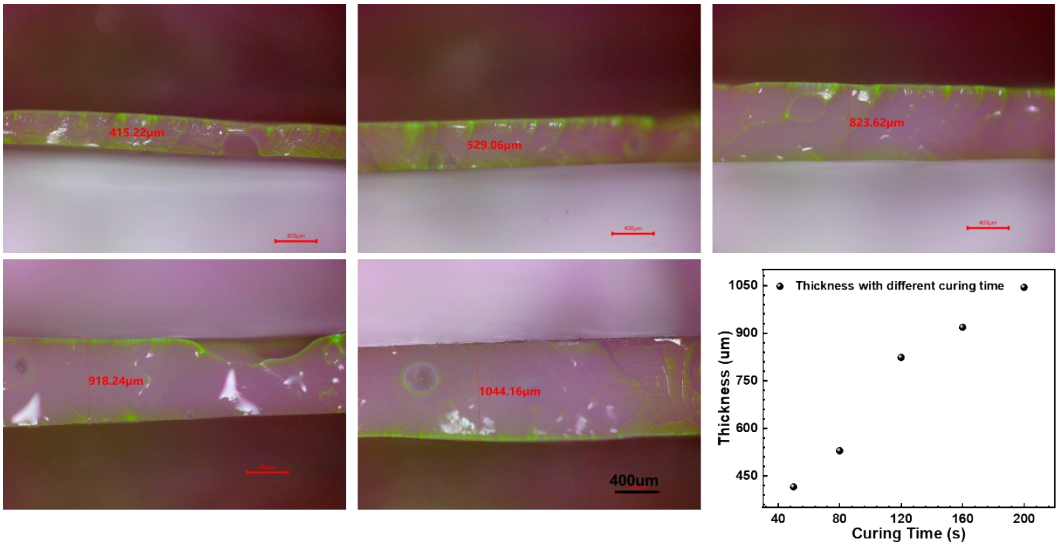

Figure S9. 3D printing curing depth for different curing times.

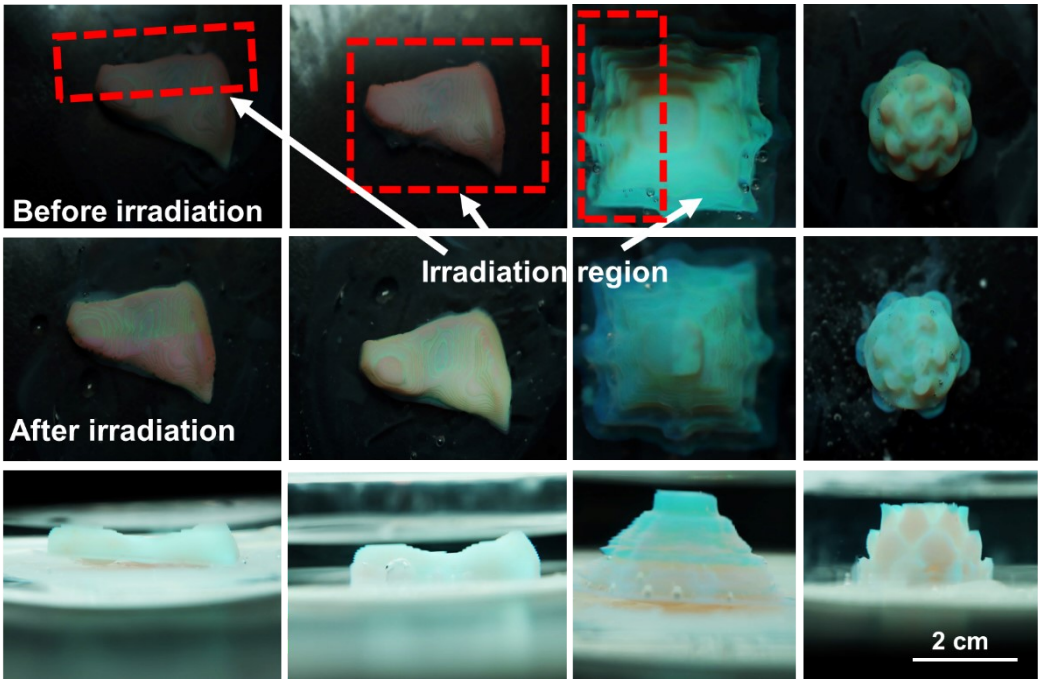

Figure S10. Photographs of 3D models before and after irradiation under different patterned radiation fields.